

Spatiotemporal Self-Organization of Fluctuating Bacterial Colonies

Tobias Grafke,¹ Michael E. Cates,² and Eric Vanden-Eijnden¹

¹*Courant Institute, New York University, 251 Mercer Street, New York, NY 10012, USA*

²*DAMTP, Centre for Mathematical Sciences, Wilberforce Road, Cambridge, CB3 0WA, United Kingdom*

(Dated: September 14, 2021)

We model an enclosed system of bacteria, whose motility-induced phase separation is coupled to slow population dynamics. Without noise, the system shows both static phase separation and a limit cycle, in which a rising global population causes a dense bacterial colony to form, which then declines by local cell death, before dispersing to re-initiate the cycle. Adding fluctuations, we find that static colonies are now metastable, moving between spatial locations via rare and strongly nonequilibrium pathways, whereas the limit cycle becomes almost periodic such that after each redispersion event the next colony forms in a random location. These results, which hint at some aspects of the biofilm-planktonic life cycle, can be explained by combining tools from large deviation theory with a bifurcation analysis in which the global population density plays the role of control parameter.

PACS numbers: 87.10.Mn, 87.17.Jj, 05.40.-a

Because they are not bound by the standard laws of equilibrium thermodynamics, active materials such as bird flocks [1], motile bacteria [2], self-organizing bio-polymers [3, 4], or man-made self-propelled particles [5] have many more routes towards self-assembly and self-organization than systems whose dynamics satisfy detailed-balance. Motility-induced phase separation (MIPS) is one example [6, 7]. MIPS arises naturally in systems of self-propelled particles whose locomotive speed decreases monotonically with density, through a feedback in which particles accumulate where they move slowly and vice-versa. This provides a generic path to pattern formation in motile agents, including both micro-organisms such as *E. coli* [8, 9], where slowdown can be caused by quorum sensing [10–13], and synthetic colloidal analogues where slowdown is caused by crowding [7, 14–17]. The simplest theories of MIPS describe phase separation through an effective free energy functional [7], although active gradient terms can alter this structure and the resulting coexistence behavior [6, 7].

MIPS, can be arrested by the birth and death of particles. The simplest (logistic) population dynamics has for uniform systems a stable fixed point at some carrying capacity ρ_0 , with decay towards this from higher or lower densities. If ρ_0 lies within the miscibility gap of a phase separation, the uniform state at ρ_0 is unstable, but so is a state of coexisting bulk phases (each of which would have nonstationary density). This can result in stationary patterns of finite wavelength, in which bacteria reproduce in dilute regions, migrate by diffusive motility to dense ones, become immotile, and there die off by overcrowding [7, 18]. In [18] a field theoretic description of such arrested phase separation was proposed to capture the variety of bacterial colony patterns earlier observed in experiments [19].

The work of [18] mainly describes stationary spatial rather than spatiotemporal patterns, and crucially neglects the effects of intrinsic fluctuations in population density and motility of the bacteria. These fluctuations are always present in finite systems and they are relevant to the nature and stability of the self-assembling structures. One purpose of the present Letter

is to explore these effects in situations where birth and death processes are slow compared to diffusive exploration times. Another is to show that entirely different physics from that reported in [18] can arise, involving spatiotemporal rather than static patterning. For simplicity we focus on one-dimensional systems whose extent is smaller than the natural length scale for the spacing between dense patches, controlled by the distance a particle can move during its lifetime. Accordingly, only one dense bacterial domain of low motility (hereafter ‘colony’) is present at a time, with the remaining bacteria in a dilute and motile (i.e., ‘planktonic’) phase. These simplifications allow us to focus on temporal aspects of the pattern formation, and also to give a thorough analysis of the role of noise terms. Our qualitative conclusions, however, apply in higher dimensions.

Concretely, we identify two regimes in which the fluctuations induce nontrivial self-organization pathways. The first arises in situations where the deterministic dynamics possess time-periodic solutions driven by the interplay between MIPS and the competition for resources: in the resulting limit cycles a colony of bacteria periodically appears and disappears at a fixed location in the domain. In this regime, the fluctuations, no matter how small, are shown to have a drastic impact: they allow the colony to explore its environment by randomly jumping from one location to another each time the system revisits its spatially homogeneous planktonic state. With periodic spatial boundary conditions the colony now appears and disappears at spatially random locations; if boundary conditions instead favor localization at container walls, a random choice of wall is made each cycle. It is striking that this behavior, which resembles the biofilm-planktonic lifecycle of several micro-organisms [20] can arise from the combination of MIPS and logistic growth alone – particularly as the bacterial quorum sensing response, a likely cause of MIPS [9, 18] is now thought also to be directly implicated in biofilm dispersion [13]. We are not suggesting that the combination of MIPS and logistic growth directly explains the complex life cycle of real biofilms, but it may nonetheless be a contributory factor in its evolution from simpler beginnings.

In the second regime, we show that the deterministic theory predicts a single static colony with multiple stable locations. In these situations the intrinsic fluctuations induce rare, noise-activated transitions via the uniform state from one such metastable pattern to another. (This again resembles the biofilm lifecycle, but now with random intervals between dispersion events.) As shown below, the rate and mechanism of these transitions can be completely characterized using tools from large deviation theory (LDT) [21]. The transition pathways are intrinsically out-of-equilibrium and involve a subtle interplay between phase-separation and reproduction. In particular these transitions do not follow the deterministic relaxation path in reverse, as one would predict from standard equilibrium arguments in systems with microscopic reversibility.

Following [18], we focus on motile bacteria whose motile diffusivity $D(\rho) = \frac{1}{2}v^2(\rho)\tau/d$ [9] depends on their local density ρ via the swim speed $v(\rho)$. Here τ is a rotational relaxation time and d is dimensionality. Because the swim speed varies in space through ρ , the particles have a mean drift velocity $\mathbf{V}(\rho) = -\frac{1}{2}D'(\rho)\nabla\rho$ [9]. Neglecting fluctuations, these effects can be combined into the following equation governing the evolution of the bacterial density $\rho(\mathbf{x}, t)$:

$$\partial_t \rho = \nabla \cdot (\mathcal{D}_e(\rho)\nabla\rho) - \delta^2 \nabla \cdot (\rho D(\rho)\nabla\Delta\rho). \quad (1)$$

In this equation the diffusivity and drift have been combined into a collective diffusivity $\mathcal{D}_e(\rho) = D(\rho) + \frac{1}{2}\rho D'(\rho)$, and a higher-order gradient, or regularizing, term proportional to δ^2 has been added to account for the fact that the bacteria only sense each other's influence over a finite distance $\delta > 0$ [22].

Our choice of regularizer is the simplest form to emerge from explicit coarse-graining of the microscopic dynamics of active particles [7, 9, 23]. With this form, and in the absence of birth-death processes, the physics of MIPS, including all noise contributions, maps exactly onto an equilibrium model of phase separation. The regularizer then derives from a square gradient contribution in an underlying free energy that describes passive Brownian particles with attractive interactions [7]. (A more detailed coarse-graining gives further gradient terms that are not representable by any free energy; these shift the MIPS phase boundaries only slightly [7, 24].) Thus our model, whose microscopic derivation is in the supplemental material [25], includes a fluctuating noise term in Eq. (1) such that its dynamics obey detailed balance (DB) with the free energy

$$E[\rho] = \int_{\Omega} (\rho \log \rho - \rho + f(\rho) + \frac{1}{2}\delta^2 |\nabla\rho|^2) d\mathbf{x}. \quad (2)$$

Eq. (1) then takes the form of a generalized gradient flow, $\partial_t \rho = -M(\rho)(\delta F/\delta\rho)$, with nonlinear mobility operator $M(\rho)\xi = \nabla \cdot (\rho D(\rho)\nabla\xi)$ [26]. The DB property of Eq. (1) is inessential since it is violated by the birth and death terms added below [27] but it simplifies the analysis when these are small. The regularizer used here is an improvement on the one adopted in [18], which is purely phenomenological and does not emerge from any known coarse-graining of an active-particle model.

Crucially, whenever $d \ln v/d \ln \rho < -1$, we have $\mathcal{D}_e(\rho) < 0$ in (1). This is the spinodal regime of local instability for MIPS [9]. We assume $v(\rho) = v_0 e^{-\lambda\rho/2}$ where v_0 is the speed of an isolated particle and $\lambda > 0$ [18]. In a d -dimensional box $\Omega = [0, L]^d$, after non-dimensionalization via $\tau v_0^2 = \lambda = 1$, (1) reduces to

$$\partial_t \rho = \nabla \cdot \left((1 - \frac{1}{2}\rho) e^{-\rho} \nabla \rho - \delta^2 \rho e^{-\rho} \Delta \nabla \rho \right). \quad (3)$$

We study (3) for $\mathbf{x} \in \Omega = [0, 1]^d$ with, unless otherwise stated, Neumann boundary conditions: $\hat{\mathbf{n}} \cdot \nabla \rho = 0 \forall \mathbf{x} \in \partial\Omega$ for $\hat{\mathbf{n}}$ normal to the boundary. These localize the dense phase at a wall, to minimize its interfacial energy.

The mean bacterial density, $\bar{\rho} = |\Omega|^{-1} \int_{\Omega} \rho(\mathbf{x}) d\mathbf{x}$, is conserved by (3) and controls the phase separation. Fig. 1 (left) shows the bifurcation diagram obtained when $d = 1$ and $\delta^2 = 2 \cdot 10^{-3}$ by projecting the fixed points of (3) onto the $(\bar{\rho}, A)$ plane, where the ‘signed asymmetry’ is defined as $A[\rho] = \int_0^{1/2} \rho(x) dx - \int_{1/2}^1 \rho(x) dx$. A linear stability analysis finds the spatially uniform solution to be stable if $\bar{\rho} < \rho_S = 2/(1 - 2\delta^2\pi^2)$. (This becomes the bulk spinodal condition in the large system, or small δ , limit.) A subcritical pitchfork bifurcation occurs at $\bar{\rho} = \rho_S$, where two unstable and one stable branches merge into a single unstable branch. The remaining two stable branches, $\rho_L(x)$ and $\rho_R(x)$, correspond to colony formation on either the left or the right wall. Once present, each such phase-separated state remains stable down to a ‘binodal’ density $\bar{\rho} = \rho_B < \rho_S$ [28], whereas for $\bar{\rho} < \rho_B$ the colony redisperses diffusively.

These transitions in static stability become *dynamically* significant once the mean bacterial density $\bar{\rho}$ is allowed to change by introducing logistic growth. Focusing again on the deterministic situation first, this adds to (3) a term $\alpha\rho(1 - \rho/\rho_0)$, where α is the birth rate and ρ_0 is the carrying capacity. Crucially, this breaks detailed balance, allowing not only steady-state fluxes [18] but also nonstationary patterns (see below). When the population dynamics is much slower than particle motion, $\alpha \ll 1$, the bifurcation diagram shown in Fig. 1 now depicts the projection of a *slow manifold* \mathcal{M} instead. Diffusive motility leads to convergence of ρ to \mathcal{M} on a fast time-scale $O(1)$ in α , during which the global mean $\bar{\rho}$ is almost conserved. On \mathcal{M} itself, the motion is driven solely by changing $\bar{\rho}$ via the slow logistic term on time-scales $O(\alpha^{-1})$.

Three different regimes can then be identified on varying the carrying capacity ρ_0 . For $\rho_0 < \rho_S$ the system remains in a uniform phase, in which dilute motile bacteria homogeneously cover the domain at $\rho(x) = \rho_0$ [29]. At higher capacities homogeneous solutions cannot exist, and the solution jumps to one of the stable branches, leading to a dense layer of immotile bacteria at one of the boundaries, which forms on the fast time-scale. However, for carrying capacities $\rho_S < \rho_0 < \rho_0^c$, the resulting colony is destabilized by the birth/death term; two limit cycles then appear. As soon as a colony emerges at one end of the domain, the bacteria in it start to slowly die out until the global density drops again to ρ_B . It then disperses rapidly, reverting to a uniform phase, whose density slowly grows until

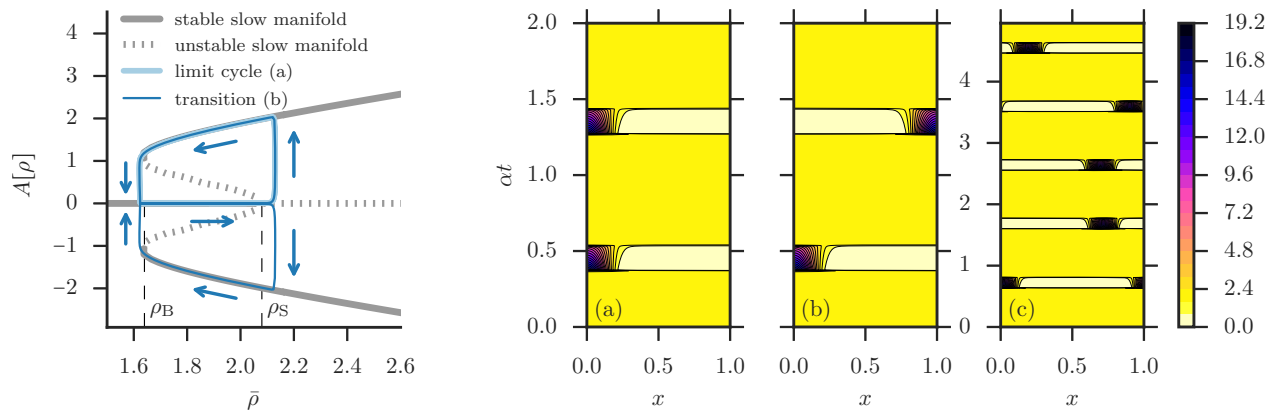


FIG. 1. *Left panel:* Bifurcation diagram in a 2-dimensional projection. The x -axis shows the spatial mean of ρ , the y -axis shows its signed asymmetry $A[\rho]$ (see text for details). For carrying capacities $\rho_S < \rho_0 < \rho_0^c$, no stable fixed point of the dynamics exist. A limit cycle (light blue) and a trajectory with a small amount of noise (dark blue) that exhibits a transition to the lower stable branch are projected into the diagram. *Right panels (a), (b), and (c):* The time-evolution of the limit cycle with a colony located at the left boundary (upper cycle on the left panel) is shown in subplot (a). Fluctuations allow the solution to randomly jump between the limit cycles with colonies located at the left or right of the domain, as shown in subplot (b). Subplot (c) depicts the almost periodic regime in a spatially periodic domain, where the fluctuations randomize the colony location.

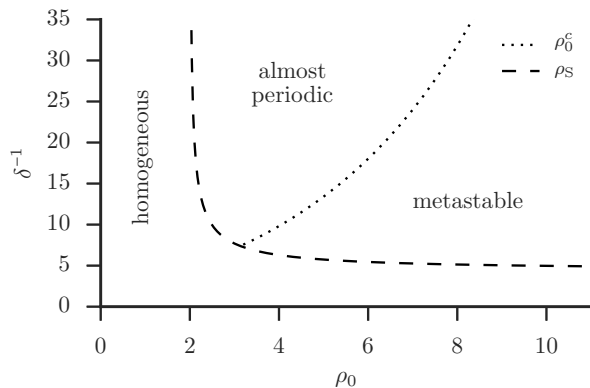


FIG. 2. Phase diagram a function of ρ_0 and δ , showing regimes with homogeneous, almost periodic, and metastable solutions. The dashed line shows $\rho_S = 2/(1 - 2\delta^2\pi^2)$, the dotted line ρ_0^c .

ρ_S is reached and the cycle begins anew. Symmetry is broken by weak memory of the previous cycle, so that the colony always reforms in the same place. (This also holds with periodic boundary conditions, but the location is then arbitrary.) One of these limit cycles is projected onto the bifurcation diagram in Fig 1 (left), and its spatio-temporal evolution shown in Fig. 1 (right, a).

Finally, for $\rho_0 > \rho_0^c$, all stable fixed points of the system comprise a dense colony in coexistence with a planktonic ‘vapor’. A steady flux of particles from the vapor balances cell-death within the colony, so that the macroscopic model is stationary, while the microscopic dynamics are not [18]. Such fixed points correspond to points on stable branches of the slow manifold \mathcal{M} . For $d = 1$ there are two such branches ($\rho_{L,R}$), with more in $d \geq 2$, corresponding to (say) colonies located

in the corners of a square in $d = 2$. For these computations and the ones below, we picked $\alpha = 10^{-4}$ and $\delta^2 = 2 \cdot 10^{-3}$, which leads to $\rho_S \approx 2.08$, $\rho_B \approx 1.64$, and $\rho_0^c \approx 6.749$. The complete phase diagram in δ and ρ_0 is shown in Fig. 2.

So far we have neglected the effect of intrinsic fluctuations, both in the diffusive and the reproductive dynamics. The fluctuations in diffusion can be formally accounted for by adding in (3) a noise-term $\sqrt{N^{-1}}\nabla \cdot (\sqrt{2\rho D(\rho)}\eta)$, where η is spatio-temporal white noise and N is the typical number of particles present in the domain Ω . On the other hand, the population dynamics can be modeled by a reversible reaction $A \leftrightarrow A + A$ with forward and backward rates $r_f = \alpha$ and $r_b = \alpha/(N\rho_0)$ [27]. The combined effect is captured by a Markov jump process. In the limit $N \rightarrow \infty$, this gives the logistic growth term $\alpha\rho(1 - \rho/\rho_0)$ considered before, with fluctuations that are Poisson at each location, scaling again with $\sqrt{N^{-1}}$ [30].

We consider only the weak fluctuation (large N) regime which can be captured by LDT [21]. This theory predicts that a noise-driven event occurs, with probability close to 1, via the path involving the least unlikely fluctuation able to drive this event. The resulting most likely path (MLP, also referred to as the *instanton*) is the minimizer of the action functional

$$I_T[\rho] = \frac{1}{2} \int_0^T dt \int_{\Omega} d\mathbf{x} \theta(\mathbf{x}, t; \rho) \partial_t \rho(\mathbf{x}, t) \quad (4)$$

which quantifies the likelihood of the ‘fluctuation’ $\theta(\mathbf{x}, t; \rho)$. In our context, $\theta(\mathbf{x}, t; \rho)$ is related to $\rho(\mathbf{x}, t)$ [25] via

$$\partial_t \rho = \nabla \cdot (D_e(\rho)\nabla \rho - \rho D(\rho)\nabla(\delta^2 \Delta \rho + 2\theta)) + \alpha \rho e^{\theta} - \alpha \rho^2 e^{-\theta} / \rho_0. \quad (5)$$

The action I_T should be minimized over all paths, and all durations T , consistent with the event of interest, giving $I^* =$

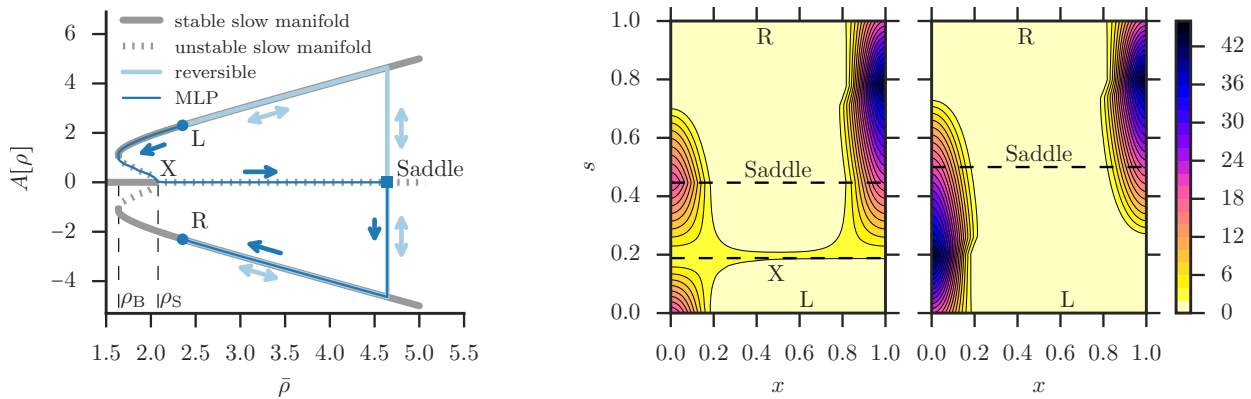


FIG. 3. Transition paths between ρ_L and ρ_R . Here, $x \in [0, 1]$ denotes the spatial extent and $s \in [0, 1]$ the normalized arc-length along each trajectory. *Left*: Projection into bifurcation diagram, see Fig. 1. *Center*: MLP from ρ_L to ρ_R . *Right*: Reversible transition from ρ_L to ρ_R .

$\inf_{T>0} \inf_{\rho} I_T[\rho]$. The minimizer is the MLP for the event, whose rate is then, up to a prefactor, $\exp(-NI^*)$ [31].

In the regime $\rho_0 < \rho_S$, the spatially homogeneous configuration is stable and LDT predicts that deviations away from it are exponentially rare and transient. This is no longer true for $\rho_S < \rho_0 < \rho_0^c$: Since part of the limit cycle tracks $O(\alpha)$ close to the separatrix for times $O(\alpha^{-1})$, even tiny fluctuations can trigger a crossing of the separatrix into the other limit cycle. This is consistent with LDT, for which in the limit $\alpha \rightarrow 0$ zero-action minimizers connect these two limit cycles. Therefore, due to the fluctuations, bacterial colonies randomly appear either on the left or right wall, disappearing again after times $O(\alpha^{-1})$. This switching behavior is depicted in Fig. 1 (b). With periodic boundary conditions, the colony instead appears at a random location each cycle, as shown in Fig. 1 (c). Note that the time period of the cycles is not affected significantly by these fluctuations.

For $\rho_0 > \rho_0^c$, on the other hand, ρ_L and ρ_R become metastable; the noise triggers rare and aperiodic transitions between them. A projection of the resulting MLP from ρ_L to ρ_R onto the bifurcation diagram is shown in Fig. 3 (left), whereas its actual shape is shown in Fig. 3 (center); that from ρ_R to ρ_L follows by symmetry. To understand its features, notice that the slow manifold connects the two stable fixed points ρ_L and ρ_R through the bifurcation point, and so can be used as a channel to facilitate the transition. This is indeed correct for $\delta \ll 1$, as the free energy barrier for a jump between stable branches scales like δ^{-1} [32]. It is confirmed by a numerical calculation of the MLP as shown in Fig. 3 (center): The colony of bacteria on the left first disperses to form a uniform planktonic phase which then attains the bifurcation point $\rho_X(x) = \rho_S$. The system then follows the unstable branch (separatrix) of \mathcal{M} – with two symmetric colonies – to the saddle point at $\rho_{\text{Saddle}}(x)$, where it enters the basin of attraction of ρ_R . Note that for finite N , diffusive noise will push the actual trajectory off the separatrix well before it reaches the transition state at ρ_{Saddle} . The event rate is still found by LDT, since the motion after visiting ρ_X is effectively deterministic and does not contribute to I^* .

Let us stress the non-equilibrium nature of this transition: If the system were in detailed balance, time-reversal symmetry would require the transition path to follow the deterministic relaxation trajectory in reverse from ρ_L to the transition state ρ_{Saddle} , and then relax deterministically to ρ_R (see Fig. 3). Along this trajectory, the colony initially grows instead of shrinking, bringing the global average density $\bar{\rho}$ up to ρ_{Saddle} . Subsequently, bacteria leave the colony, cross the low-density region in the center, and accumulate on the opposite wall, keeping $\bar{\rho}$ constant. This part of the transition happens diffusively causing the system to leave the slow manifold. After passing through ρ_{Saddle} , the reversible transition necessarily coincides with the true MLP.

In summary, we have analyzed a minimal model for the fluctuating dynamics of self-organization among motile bacteria in a finite domain, in the presence of birth and death processes that are slow compared to diffusive time-scales. For $\rho_S < \rho_0 < \rho_0^c$, a bacterial colony is present; fluctuations allow it to explore the domain by random relocation at regular intervals. This exploration remains possible at higher carrying capacities, $\rho_0 > \rho_0^c$, where fluctuations now induce exponentially rare, aperiodic relocations. Such transitions are inherently out-of-equilibrium: their most likely path differs significantly from the one followed in systems with time-reversible dynamics. In our model, relocation of a colony is triggered by a slow decline in local population density, followed by rapid dispersal and re-formation elsewhere, rather than by progressive migration between old and new sites. The intermediate state has no colonies in the first case and two in the second – alternatives that should be clearly distinguishable experimentally. Similar considerations may apply to other organisms that alternate between nomadic and cooperative lifestyles. The formalism readily applies to a higher-dimensional setup, e.g. bacterial colonies in the corners of a two-dimensional rectangular domain, and a slow manifold with four stable branches.

Acknowledgments. We thank T. Schäfer for his help with the numerical scheme and A. Donev, O. Hirschberg, and C. Nardini for interesting discussions. MEC is funded by the

Royal Society. EVE is supported in part by the Materials Research Science and Engineering Center (MRSEC) program of the National Science Foundation (NSF) under award number DMR-1420073 and by NSF under award number DMS-1522767.

-
- [1] M. Ballerini, N. Cabibbo, R. Candelier, A. Cavagna, E. Cisbani, I. Giardina, V. Lecomte, A. Orlandi, G. Parisi, A. Procaccini, M. Viale, and V. Zdravkovic, *Proceedings of the National Academy of Sciences* **105**, 1232 (2008).
- [2] M. C. Marchetti, J. F. Joanny, S. Ramaswamy, T. B. Liverpool, J. Prost, M. Rao, and R. A. Simha, *Reviews of Modern Physics* **85**, 1143 (2013).
- [3] V. Schaller, C. Weber, C. Semmrich, E. Frey, and A. R. Bausch, *Nature* **467**, 73 (2010).
- [4] Y. Sumino, K. H. Nagai, Y. Shitaka, D. Tanaka, K. Yoshikawa, H. Chaté, and K. Oiwa, *Nature* **483**, 448 (2012).
- [5] J. R. Howse, R. A. L. Jones, A. J. Ryan, T. Gough, R. Vafabakhsh, and R. Golestanian, *Physical Review Letters* **99**, 048102 (2007).
- [6] R. Wittkowski, A. Tiribocchi, J. Stenhammar, R. J. Allen, D. Marenduzzo, and M. E. Cates, *Nature Communications* **5**, 4351 (2014).
- [7] M. E. Cates and J. Tailleur, *Annual Review of Condensed Matter Physics* **6**, 219 (2015).
- [8] J. A. Shapiro, *BioEssays* **17**, 597 (1995).
- [9] J. Tailleur and M. E. Cates, *Physical Review Letters* **100**, 218103 (2008).
- [10] M. R. Parsek and E. P. Greenberg, *Trends in Microbiology* **13**, 27 (2005).
- [11] C. Liu, X. Fu, L. Liu, X. Ren, C. K. L. Chau, S. Li, L. Xiang, H. Zeng, G. Chen, L.-H. Tang, P. Lenz, X. Cui, W. Huang, T. Hwa, and J.-D. Huang, *Science* **334**, 238 (2011).
- [12] X. Fu, L.-H. Tang, C. Liu, J.-D. Huang, T. Hwa, and P. Lenz, *Physical Review Letters* **108**, 198102 (2012).
- [13] C. Solano, M. Echeverez, and I. Lasa, *Current Opinion in Microbiology Cell regulation*, **18**, 96 (2014).
- [14] Y. Fily and M. C. Marchetti, *Physical Review Letters* **108**, 235702 (2012).
- [15] J. Palacci, S. Sacanna, A. P. Steinberg, D. J. Pine, and P. M. Chaikin, *Science* **339**, 936 (2013).
- [16] I. Buttinoni, J. Bialké, F. Kümmel, H. Löwen, C. Bechinger, and T. Speck, *Physical Review Letters* **110**, 238301 (2013).
- [17] M. E. Cates and J. Tailleur, *EPL (Europhysics Letters)* **101**, 20010 (2013).
- [18] M. E. Cates, D. Marenduzzo, I. Pagonabarraga, and J. Tailleur, *Proceedings of the National Academy of Sciences* **107**, 11715 (2010).
- [19] J. Murray, *Mathematical Biology II: Spatial Models and Biochemical Applications, volume II* (Springer-Verlag, 2003).
- [20] M. Kostakioti, M. Hadjifrangiskou, and S. J. Hultgren, *Cold Spring Harbor Perspectives in Medicine* **3**, a010306 (2013).
- [21] M. I. Freidlin and A. D. Wentzell, *Random perturbations of dynamical systems*, Vol. 260 (Springer, 2012).
- [22] In general this effect leads to a nonlocal equation, out of which (1) emerges at leading order after expansion in $\delta \ll 1$ [32].
- [23] T. Speck, J. Bialké, A. M. Menzel, and H. Löwen, *Physical Review Letters* **112**, 218304 (2014).
- [24] J. Stenhammar, A. Tiribocchi, R. J. Allen, D. Marenduzzo, and M. E. Cates, *Physical Review Letters* **111**, 145702 (2013).
- [25] See supplemental material at [URL will be inserted by publisher] for a derivation from a microscopic model.
- [26] A. Mielke, D. R. M. Renger, and M. A. Peletier, *Journal of Non-Equilibrium Thermodynamics* **41**, 141 (2016).
- [27] Detailed balance violation arises because the rates for birth and death are unaffected by the motility induced “attractions” (whose true origin is kinetic) whereas genuine enthalpic attractions would require the birth and death rates to become explicitly density dependent [33–36].
- [28] For the particular choice in (3), $\rho_B \rightarrow 0$ in the large system limit but for a finite system the lower stability limit $\rho_B < \rho_S$ remains nonzero, albeit now depending on $\bar{\rho}$ as well as δ .
- [29] Note that for $\rho_B < \rho_0 < \rho_S$, the two phase separated states $\rho_{L,R}$ are destabilized by the α term.
- [30] A. Shwartz and A. Weiss, *Large Deviations For Performance Analysis: Queues, Communication and Computing* (CRC Press, 1995).
- [31] The numerical details of the minimization are discussed in [37, 38].
- [32] T. Grafke, O. Hirschberg, and E. Vanden-Eijnden, “Stochastic thermodynamics of reproducing, motile bacteria,” (2017), in preparation.
- [33] R. Lefever, D. Carati, and N. Hassani, *Physical Review Letters* **75**, 1674 (1995).
- [34] S. C. Glotzer, E. A. Di Marzio, and M. Muthukumar, *Physical Review Letters* **74**, 2034 (1995).
- [35] S. C. Glotzer, D. Stauffer, and N. Jan, *Physical Review Letters* **72**, 4109 (1994).
- [36] S. C. Glotzer, D. Stauffer, and N. Jan, *Physical Review Letters* **75**, 1675 (1995).
- [37] M. Heymann and E. Vanden-Eijnden, *Communications on Pure and Applied Mathematics* **61**, 1052 (2008).
- [38] T. Grafke, T. Schäfer, and E. Vanden-Eijnden, arXiv:1604.03818 [cond-mat] (2016)
- The following reference appears in the supplemental material .**
- [39] L. Bertini, A. De Sole, D. Gabrielli, G. Jona-Lasinio, and C. Landim, *Reviews of Modern Physics* **87**, 593 (2015).

SUPPLEMENTAL MATERIAL: SPATIOTEMPORAL SELF-ORGANIZATION OF FLUCTUATING BACTERIAL COLONIES

TOBIAS GRAFKE, MICHAEL E. CATES, AND ERIC VANDEN-EIJNDEN

Below we give some additional details about the derivation of the equations given in main text, and in particular explain: (i) how to obtain a spatially-continuous model from a microscopic description of the microorganisms based on a lattice gas model, and (ii) how to account for the effects of fluctuations at continuous level using a large deviation principle (LDP).

1. Motile microorganisms modeled as lattice gas. We model the behavior of spatially extended bacterial colonies as a Markov jump process (MJP) of particles on a one-dimensional lattice with L sites of physical width $h = 1/L$, i.e. such that the extent of the physical domain Ω is normalized to $\Omega = [0, 1]$ – the generalization to multidimensional domains is straightforward but makes the notations more cumbersome so we avoid it here. We assume that there exist two sub-populations moving left or right, and denote by n_i^- the number of left-moving particles at site i and by n_i^+ the number of right-moving particles at site i . We use the vectors $\mathbf{n}^\pm = (n_1^\pm, \dots, n_L^\pm) \in \mathbb{N}^L$ to describe the complete configuration of all the particles in the domain. We assume that the rates of hopping from site i to site $i - 1$ (for the left-moving particles) or site i to site $i + 1$ (for the right-moving particles) are the same and depend on the total number of particles at site i : $n_i = n_i^- + n_i^+$ (*quorum sensing*). Denoting this common rate by $v(n_i)$, the statistical evolution of any observable $f(t, \mathbf{n}_0^-, \mathbf{n}_0^+) \equiv \mathbb{E}(\phi(\mathbf{n}^-(t), \mathbf{n}^+(t)) | \mathbf{n}^-(0) = \mathbf{n}_0^-, \mathbf{n}^+(0) = \mathbf{n}_0^+)$ can be described by the backward Kolmogorov equation (BKE),

$$\partial_t f(t, \mathbf{n}^-, \mathbf{n}^+) = L_{\text{prop}} f(t, \mathbf{n}^-, \mathbf{n}^+), \quad f(0, \mathbf{n}^-, \mathbf{n}^+) = \phi(\mathbf{n}^-, \mathbf{n}^+), \quad (\text{SM.1})$$

where L_{prop} is the generator of the MJP (we use the subscript ‘prop’ to distinguish this propulsion part of the generator with the reproduction part considered below):

$$\begin{aligned} L_{\text{prop}} f(t, \mathbf{n}^-, \mathbf{n}^+) &= \sum_{i=1}^L n_i^+ v(n_i) (f(t, \mathbf{n}^-, \mathbf{n}^+ + \mathbf{e}_i^+) - f(t, \mathbf{n}^-, \mathbf{n}^+)) && \text{(right jumps)} \\ &+ \sum_{i=1}^L n_i^- v(n_i) (f(t, \mathbf{n}^- + \mathbf{e}_i^-, \mathbf{n}^+) - f(t, \mathbf{n}^-, \mathbf{n}^+)) && \text{(left jumps)} \\ &+ \tau^{-1} \sum_{i=1}^L n_i^- (f(t, \mathbf{n}^- - \mathbf{e}_i, \mathbf{n}^+ + \mathbf{e}_i) - f(t, \mathbf{n}^-, \mathbf{n}^+)) && \text{(tumbles right to left)} \\ &+ \tau^{-1} \sum_{i=1}^L n_i^+ (f(t, \mathbf{n}^- + \mathbf{e}_i, \mathbf{n}^+ - \mathbf{e}_i) - f(t, \mathbf{n}^-, \mathbf{n}^+)) && \text{(tumbles left to right)} \end{aligned} \quad (\text{SM.2})$$

Here τ defines the tumbling rate and

$$\mathbf{e}_i^+ = (0, \dots, 0, \underbrace{-1}_i, \underbrace{1}_{i+1}, 0, \dots, 0), \quad \mathbf{e}_i^- = (0, \dots, 0, \underbrace{1}_{i-1}, \underbrace{-1}_i, 0, \dots, 0), \quad \mathbf{e}_i = (0, \dots, 0, \underbrace{1}_i, 0, \dots, 0). \quad (\text{SM.3})$$

The particular form of the rate v depends on physical considerations on the model of the motility of the random walkers. Later on, we will add non-locality to the rate to realize quorum sensing. In the next section, we are going to make this model continuous, first by considering the large number of particle limit and then by taking the continuous limit in space.

1.1. Derivation of the continuous model from the microscopic model. Let N be a typical number of particles in the domain. Denote by $\rho_i^\pm = Ln_i^\pm/N$ the particle density at site i . This choice would yield a normalization $h \sum_i \rho_i = 1$ if we had $\sum_i n_i = N$, but since we later add reproduction to the model the total number of particles is not conserved and N is

merely a scaling parameter. By writing $\epsilon = L/N$, and redefining the functions f and v appropriately, the BKE becomes

$$\begin{aligned}
\partial_t f(t, \boldsymbol{\rho}, \boldsymbol{\eta}) &= \frac{1}{\epsilon} \sum_{i=0}^L \rho_i^+ v(\rho_i) (f(t, \boldsymbol{\rho}^-, \boldsymbol{\rho}^+ + \epsilon \mathbf{e}_i^+) - f(t, \boldsymbol{\rho}^-, \boldsymbol{\rho}^+)) && \text{(right jumps)} \\
&+ \frac{1}{\epsilon} \sum_{i=0}^L \rho_i^- v(\rho_i) (f(t, \boldsymbol{\rho}^- + \epsilon \mathbf{e}_i^-, \boldsymbol{\rho}^+) - f(t, \boldsymbol{\rho}^-, \boldsymbol{\rho}^+)) && \text{(left jumps)} \\
&+ \frac{1}{\epsilon \tau} \sum_{i=1}^L \rho_i^- (f(t, \boldsymbol{\rho}^- - \epsilon \mathbf{e}_i, \boldsymbol{\rho}^+ + \epsilon \mathbf{e}_i) - f(t, \boldsymbol{\rho}^-, \boldsymbol{\rho}^+)) && \text{(tumbles right to left)} \\
&+ \frac{1}{\epsilon \tau} \sum_{i=1}^L \rho_i^+ (f(t, \boldsymbol{\rho}^- + \epsilon \mathbf{e}_i, \boldsymbol{\rho}^+ - \epsilon \mathbf{e}_i) - f(t, \boldsymbol{\rho}^-, \boldsymbol{\rho}^+)) . && \text{(tumbles left to right)}
\end{aligned} \tag{SM.4}$$

In order to consider the large particle limit, we let $\epsilon \rightarrow 0$, that is, we assume that the number of particles per cell is large. At the same time, we make a WKB ansatz, i.e. we set $f(t, \boldsymbol{\rho}^-, \boldsymbol{\rho}^+) = \exp(S(t, \boldsymbol{\rho}^-, \boldsymbol{\rho}^+)/\epsilon)$. This will allow us to derive a large deviation principle (LDP) for the stochastic system [21, 30], while avoiding introducing stochastic partial differential equations (SPDEs), which from a mathematical perspective are ill-defined in the continuous space limit $h \rightarrow 0$ due to the multiplicative spatio-temporal white noise and the Poisson-process for the reaction terms. To leading order in ϵ the function S satisfies the following Hamilton-Jacobi equation (HJE):

$$\partial_t S(t, \boldsymbol{\rho}^-, \boldsymbol{\rho}^+) = H(\boldsymbol{\rho}^-, \boldsymbol{\rho}^+, \nabla_{\boldsymbol{\rho}^-} S, \nabla_{\boldsymbol{\rho}^+} S) \tag{SM.5}$$

with the Hamiltonian

$$\begin{aligned}
H(\boldsymbol{\rho}^-, \boldsymbol{\rho}^+, \boldsymbol{\theta}^-, \boldsymbol{\theta}^+) &= \sum_{i=1}^L \left(\rho_i^- v(\rho_i) \left(e^{\theta_{i-1}^- - \theta_i^-} - 1 \right) + \rho_i^+ v(\rho_i) \left(e^{\theta_{i+1}^+ - \theta_i^+} - 1 \right) \right) && \text{(jumps)} \\
&+ \tau^{-1} \sum_{i=0}^L \left(\rho_i^- \left(e^{\theta_i^+ - \theta_i^-} - 1 \right) + \rho_i^+ \left(e^{-\theta_i^+ + \theta_i^-} - 1 \right) \right) . && \text{(tumbles)}
\end{aligned} \tag{SM.6}$$

Next, we take the continuous space limit, i.e. let $L \rightarrow \infty$ or equivalently $h \rightarrow 0$. To this end, we define $x_i = ih$ and the spatially dependent functions $\rho^\pm(x)$ through $\rho^\pm(x_i) = \rho_i^\pm$ and similarly $\theta^\pm(x)$ through $\theta^\pm(x_i) = \theta_i^\pm$. If we rescale time according to $t \rightarrow ht$ and rescale $u \rightarrow v/h$, in the limit as $h \rightarrow 0$ the sums converges to integrals, and the HJE above converges to the functional HJE

$$\partial_t \mathcal{S}(t, \rho^-, \rho^+) = \mathcal{H}(\rho^-, \rho^+, \delta \mathcal{S} / \delta \rho^-, \delta \mathcal{S} / \delta \rho^+) \tag{SM.7}$$

with the continuous Hamiltonian

$$\begin{aligned}
\mathcal{H}[\rho^-, \rho^+, \theta^-, \theta^+] &= \int_{\Omega} (-\rho^- v(\rho) \partial_x \theta^- + \rho^+ v(\rho) \partial_x \theta^+) dx && \text{(jumps)} \\
&+ \tau^{-1} \int_{\Omega} \left(\rho^- (e^{-\theta^- + \theta^+} - 1) + \rho^+ (e^{\theta^- - \theta^+} - 1) \right) dx . && \text{(tumbles)}
\end{aligned} \tag{SM.8}$$

The functional HJE (SM.7) can be given a precise meaning via its associated Hamilton's equations (which are partial differential equation (PDEs) for ρ^\pm and θ^\pm), as described below. The HJE also permits to derive a law of large number (LLN) and a large deviation principle (LDP), which in turns allow one to describe the effect of fluctuations in the system in the large particle number and spatially-continuous limits, see Sec. 4. Here we will derive the corresponding equations in a regime where the tumbling occurs on a fast time scale, i.e. when $\tau \rightarrow 0$.

1.2. Averaging out the tumbling. In the fast tumbling limit when $\tau \rightarrow 0$, we can obtain a closed effective HJE for the total density of particles, since differences between the densities of left and right-movers are averaged out after times order $O(\tau)$. To derive this effective equation, we rescale time as $t \rightarrow t/\tau$ and introduce the variables $\rho = \rho^+ + \rho^-$ and $\eta = \eta^+ - \eta^-$, in terms of which the functional HJE (SM.7) becomes

$$\partial_t \mathcal{S}(t, \rho, \eta) = \mathcal{H}(\rho, \eta, \delta \mathcal{S} / \delta \rho, \delta \mathcal{S} / \delta \eta) \tag{SM.9}$$

for the Hamiltonian

$$\begin{aligned}
\mathcal{H}[\rho, \eta, \theta, \zeta] &= \int_{\Omega} (\eta v(\rho) \partial_x \theta + \rho v(\rho) \partial_x \zeta) dx \\
&+ \tau^{-1} \int_{\Omega} \left(\frac{1}{2} \rho (e^{2\zeta} + e^{-2\zeta} - 2) + \frac{1}{2} \eta (e^{-2\zeta} - e^{2\zeta}) \right) dx .
\end{aligned} \tag{SM.10}$$

This is equivalent to making the following canonical transformation on the Hamilton's equations associated with (SM.7)

$$\rho = \rho^+ + \rho^-, \quad \eta = \rho^+ - \rho^-, \quad \theta = \frac{1}{2}(\theta^+ + \theta^-), \quad \zeta = \frac{1}{2}(\theta^+ - \theta^-), \tag{SM.11}$$

which transform them into (these are Hamilton's equations associated with (SM.9))

$$\begin{cases} \partial_t \rho = \delta H / \delta \theta = -\tau^{-1} \partial_x (v(\rho) \eta) \\ \partial_t \eta = \delta H / \delta \zeta = -\tau^{-1} \partial_x (v(\rho) \rho) + \tau^{-2} \rho (e^{2\zeta} - e^{-2\zeta}) - \tau^{-2} \eta (e^{2\zeta} + e^{-2\zeta}) \\ \partial_t \theta = -\delta H / \delta \rho = -\tau^{-1} (\rho v'(\rho) + v(\rho)) \partial_x \zeta - \tau^{-1} \eta v'(\rho) \partial_x \theta - \frac{1}{2} \tau^{-2} (e^{2\zeta} + e^{-2\zeta} - 2) \\ \partial_t \zeta = -\delta H / \delta \eta = -\tau^{-1} v(\rho) \partial_x \theta - \frac{1}{2} \tau^{-2} (e^{-2\zeta} - e^{2\zeta}) . \end{cases} \quad (\text{SM.12})$$

We look for solutions of these equations scaling like $\eta \sim O(\tau)$, $\zeta \sim O(\tau)$, which is the correct scaling to get a limiting set of equations when tumbling is fast and the difference of populations of left and right-movers scales like τ . To this end, we replace $\eta \rightarrow \tau \eta$ and $\zeta \rightarrow \tau \zeta$ in (SM.12), expand in powers of τ , and collect terms of the same order. To leading order, $O(\tau^{-1})$, the second and fourth equation in (SM.12) give

$$\begin{cases} 0 = -\partial_x (v(\rho) \rho) + 4\rho \zeta - 2\eta \\ 0 = -v(\rho) \partial_x \theta + 2\zeta \end{cases} \quad (\text{SM.13})$$

which implies that

$$\begin{cases} \eta = -\frac{1}{2} \partial_x (v(\rho) \rho) + 2\rho \zeta = -\frac{1}{2} \partial_x (v(\rho) \rho) + \rho v(\rho) \partial_x \theta \\ \zeta = \frac{1}{2} v(\rho) \partial_x \theta . \end{cases} \quad (\text{SM.14})$$

By re-inserting (SM.14) into (SM.9) and using (SM.10), we obtain the following limiting HJE on the time scale where the tumbling has been averaged out

$$\partial_t \mathcal{S}(t, \rho) = \mathcal{H}(\rho, \delta \mathcal{S} / \delta \rho) \quad (\text{SM.15})$$

with the limiting Hamiltonian

$$\mathcal{H}[\rho, \theta] = \frac{1}{2} \int_{\Omega} (\partial_x (v(\rho) \partial_x (v(\rho) \rho)) \theta + \rho v^2(\rho) (\partial_x \theta)^2) dx \quad (\text{SM.16})$$

If we define $D(\rho) = \frac{1}{2} v^2(\rho)$ so that $v(\rho) v'(\rho) = D'(\rho)$, this limiting Hamiltonian can be rewritten as

$$\mathcal{H}[\rho, \theta] = \int_{\Omega} (\partial_x ((D(\rho) + \frac{1}{2} \rho D'(\rho)) \partial_x \rho) \theta + \rho D(\rho) (\partial_x \theta)^2) dx , \quad (\text{SM.17})$$

which yields an effective diffusivity

$$\mathcal{D}_e(\rho) = D(\rho) + \frac{1}{2} \rho D'(\rho) . \quad (\text{SM.18})$$

The corresponding Hamilton's equations are also the limiting equations obtained by inserting (SM.14) into the first and third equations in (SM.12). They read

$$\begin{cases} \partial_t \rho = \partial_x (\mathcal{D}_e(\rho) \partial_x \rho) - 2 \partial_x (\rho D(\rho) \partial_x \theta) \\ \partial_t \theta = \mathcal{D}_e(\rho) \partial_x^2 \theta + (D(\rho) + \rho D'(\rho)) (\partial_x \theta)^2 . \end{cases} \quad (\text{SM.19})$$

Note that these equations are ill-posed if $\mathcal{D}_e(\rho) < 0$. This is precisely the situation of interest to us, since it is the one that leads to MIPS. In order to regularize (SM.15) and the associated (SM.19), we introduce next a physical length scale over which the particles feel each other.

2. Quorum sensing and non-locality. Up to now, the propulsion speed of the active particles, $v(\rho)$, was set to depend on the local particle density ρ . In this section we additionally want to modify the quorum sensing by introducing a physical length scale δ over which the active walkers feel each other's influence. In effect, the jump rates v are taken to depend not only of the number of particles at the local lattice site, but also of that number at neighboring sites. To achieve this on the level of the lattice gas, we choose a fraction δ of the the physical domain $[0, 1]$ and introduce a set of coefficients $\{a_k^\delta\}_{k \in \mathbb{N}}$ with $a_k^\delta = a_{-k}^\delta$ that decay to zero fast for $|k| > \delta L$. We then make the jump rate of particles at the site i to be $v(n_i^\delta)$ instead of $v(n_i)$, where

$$n_i^\delta = \sum_{j=0}^L h a_{i-j}^\delta n_j . \quad (\text{SM.20})$$

To take the continuous limit $h \rightarrow 0$, we define a mollifier $\phi^\delta(x)$ through $\phi^\delta(x_i) = a_i^\delta$ and denote $\rho_i^\delta = L n_i^\delta / N$ to rewrite the equation above as

$$\rho_i^\delta = \sum_{j=1}^L h a_{i-j}^\delta \rho_j = \sum_{j=1}^L h \phi^\delta(x_i - x_j) \rho(x_j) \quad (\text{SM.21})$$

In the limit $h \rightarrow 0$ this Riemann sum converges to

$$\rho^\delta(x) \equiv \int_{\Omega} \phi^\delta(x-y) \rho(y) dy = \int_{\Omega} \phi^\delta(y-x) \rho(y) dy , \quad (\text{SM.22})$$

i.e. a convolution of the density field $\rho(x)$ with a mollifier of scale δ , and the jump rates are now taken as $v(\rho^\delta)$. With this modification, the Hamiltonian (SM.17) to be used in the HJE (SM.15) then becomes

$$\mathcal{H}[\rho, \theta] = \int_{\Omega} \left(\partial_x (D(\rho^\delta) \partial_x \rho + \frac{1}{2} \rho D'(\rho^\delta) \partial_x \rho^\delta) \theta + \rho D(\rho^\delta) (\partial_x \theta)^2 \right) dx. \quad (\text{SM.23})$$

Unlike (SM.19) the Hamilton's equations associated with the HJE with this Hamiltonian are well-posed even if $\mathcal{D}_e(\rho) < 0$.

2.1. *Thermodynamic mapping of the diffusive dynamics.* Let us investigate the conditions necessary to map the stochastic process defined above to a thermal system that obeys *detailed balance* (aka microscopic reversibility). Detailed balance is fulfilled if all forces derive from a free energy $E[\rho]$, and diffusion and mobility operators obey Einstein's relations, i.e. we can write the Hamiltonian in the form

$$\mathcal{H}[\rho, \theta] = -\langle \mathcal{M}[\rho] \delta E[\rho] / \delta \rho, \theta \rangle + \langle \theta, \mathcal{M}[\rho] \theta \rangle, \quad (\text{SM.24})$$

for a free energy $E[\rho]$ and a mobility operator $\mathcal{M}[\rho]$, where $\langle \cdot, \cdot \rangle$ is the $L^2(\Omega)$ inner product [39]. It is easy to see that (SM.23) can be written in the form of (SM.24) if (i) we set

$$M[\rho] \xi = -\partial_x (\rho D(\rho^\delta) \partial_x \xi) \quad (\text{SM.25})$$

for the mobility and (ii) we choose

$$E[\rho] = \int_{\Omega} (\rho \log \rho - \rho) dx + F_{\text{ex}}[\rho] \quad (\text{SM.26})$$

for the energy, with the excess free energy F_{ex} defined through

$$\frac{\delta F_{\text{ex}}[\rho]}{\delta \rho} = \frac{1}{2} \log(D(\rho^\delta)). \quad (\text{SM.27})$$

This procedure is referred to as *thermodynamic mapping* in [9]. If it can be achieved, then the stationary solution to the HJE, that is, the solution to

$$0 = H[\rho, \delta \mathcal{S} / \delta \rho] \quad (\text{SM.28})$$

is simply $\mathcal{S}[\rho] = E[\rho]$. This in turns is consistent with the equilibrium measure of the process being proportional to $\exp(-\epsilon^{-1} E[\rho])$ (i.e. to the Boltzmann-Gibbs measure), as expected for a process in detailed-balance, but it gives a precise meaning within large deviation theory (LDT) to this measure which may be ill-defined in the continuous setting.

Remembering that $\rho^\delta(x)$ is given by (SM.22), it turns out that only a specific choice of $D(\rho^\delta)$ can fulfill the equation (SM.27), i.e. allow $\log(D(\rho^\delta))$ to be written as a functional gradient. This can be demonstrated by realizing that the functional second derivative has to be symmetric, i.e. we must have

$$\frac{\delta}{\delta \rho(x)} \left(\frac{\delta F_{\text{ex}}}{\delta \rho(y)} \right) = \frac{\delta}{\delta \rho(y)} \left(\frac{\delta F_{\text{ex}}}{\delta \rho(x)} \right).$$

Since, by (SM.27),

$$\frac{\delta}{\delta \rho(x)} \left(\frac{\delta F_{\text{ex}}}{\delta \rho(y)} \right) = \frac{1}{2} \frac{\delta}{\delta \rho(x)} \log(D(\rho^\delta(y))) = \frac{1}{2} \frac{D'(\rho^\delta(y))}{D(\rho^\delta(y))} \frac{\delta \rho^\delta(y)}{\delta \rho(x)} = \frac{1}{2} \frac{D'(\rho^\delta(y))}{D(\rho^\delta(y))} \phi^\delta(x-y)$$

we see that we must have $D'(\rho^\delta)/D(\rho^\delta) = \text{cst.}$, or equivalently,

$$D(\rho^\delta) = e^{-\lambda \rho^\delta}, \quad (\text{SM.29})$$

i.e. exponential decay of the density dependent diffusivity. We choose $\lambda = 1$. For this choice, we have

$$F_{\text{ex}}[\rho] = -\frac{1}{4} \lambda \int_{\Omega} \rho \rho^\delta dx \quad \text{and} \quad E[\rho] = \int_{\Omega} \left(\rho \log \rho - \rho - \frac{1}{4} \rho \rho^\delta \right) dx. \quad (\text{SM.30})$$

In the following, for most concrete computations, we will therefore assume the form (SM.29). Note that [18] does assume the exponential form (SM.29) but combines this with a phenomenological nonlocal/gradients contribution that differs from the one found here by explicit coarse-graining. Our approach is clearly preferable.

2.2. *Regularizing surface term.* Due to the way density-dependent motility is modeled in the microscopic models, all effective equations obtained above are non-local integro-differential equations. Under the assumption that the length scale associated with the quorum sensing is small compared to the length of the domain, $\delta \ll 1$, it is possible to expand in δ to arrive at purely local models, where the nonlocal mechanism is transformed into a fourth-order regularizing surface tension term. In contrast to [18], the regularizing term introduced in this section is consistent with the thermodynamic mapping discussed above.

With the choice $\phi^\delta(x) = \frac{1}{2\sqrt{2\pi}\delta} e^{-\frac{1}{8}x^2/\delta^2}$ or in Fourier space $\hat{\phi}^\delta(k) = e^{-2k^2\delta^2}$, we can expand the convolution for $\delta \ll 1$ to obtain an expansion

$$\hat{\phi}^\delta(k) = 1 - 2k^2\delta^2 + \mathcal{O}(\delta^4).$$

As a consequence,

$$\rho^\delta(x) = \rho(x) + 2\delta^2\partial_x^2\rho(x) + \mathcal{O}(\delta^4),$$

which implies that, to $\mathcal{O}(\delta^4)$,

$$E[\rho] = \int_{\Omega} \left(\rho \log \rho - \rho - \frac{1}{4}\rho^2 + \frac{1}{2}\delta^2|\partial_x\rho|^2 \right) dx \quad (\text{SM.31})$$

as the effective free energy. Similarly, we have $D(\rho^\delta) = D(\rho) + 2\delta^2 D'(\rho)\partial_x^2\rho + \mathcal{O}(\delta^4)$, which implies that, to leading order in δ , the mobility is given by

$$M[\rho]\xi = \partial_x(\rho D(\rho)\partial_x\xi). \quad (\text{SM.32})$$

Using (SM.31) and (SM.32) in (SM.24) leads to the Hamiltonian:

$$\mathcal{H}[\rho, \theta] = \int_{\Omega} \theta \partial_x \left(\mathcal{D}_e(\rho)\partial_x\rho - \rho D(\rho)(\delta^2\partial_x^2\rho + \theta) \right) dx. \quad (\text{SM.33})$$

The corresponding LLN obtained by setting $\theta = 0$ in $\partial_t\rho = \delta\mathcal{H}/\delta\theta$ recovers equation (1) in the main text.

3. **Birth and death.** Additionally, bacteria reproduce and compete for resources. This mechanism can be represented locally as a continuous time MJP with two reactions: with a rate α , a particle, regardless of its orientation, splits into two, modeling the reproduction of the bacteria. With a rate $\alpha n_i/n_0$, one particle is annihilated, modeling the competition of bacteria for resources. Note that left and right-movers compete for the same resource with total carrying capacity n_0 . Here, α defines the time scale of the reproduction. Going back to the microscopic description in terms of \mathbf{n}^\pm , the reproduction part of the MJP is characterized by adding the following component to the generator (SM.2) entering the BKE (SM.1)

$$\begin{aligned} L_{\text{rep}}f(t, \mathbf{n}^-, \mathbf{n}^+) &= \alpha \sum_{i=0}^L (n_i^+ (f(t, \mathbf{n}^-, \mathbf{n}^+ + \mathbf{e}_i) - f(t, \mathbf{n}^-, \mathbf{n}^+))) && \text{(birth of right-mover)} \\ &+ \alpha \sum_{i=0}^L (n_i^- (f(t, \mathbf{n}^- + \mathbf{e}_i, \mathbf{n}^+) - f(t, \mathbf{n}^-, \mathbf{n}^+))) && \text{(birth of left-mover)} \\ &+ \alpha \sum_{i=0}^L \left(\frac{n_i^+ (n_i - 1)}{n_0} (f(t, \mathbf{n}^-, \mathbf{n}^+ - \mathbf{e}_i) - f(t, \mathbf{n}^-, \mathbf{n}^+)) \right) && \text{(death of right-mover)} \\ &+ \alpha \sum_{i=0}^L \left(\frac{n_i^- (n_i - 1)}{n_0} (f(t, \mathbf{n}^- - \mathbf{e}_i, \mathbf{n}^+) - f(t, \mathbf{n}^-, \mathbf{n}^+)) \right) && \text{(death of left-mover)} \end{aligned} \quad (\text{SM.34})$$

where the factors $(n_i - 1)$ in the death terms appear because a particle does not contribute to its own competition and at least two particles need to meet in order for annihilation to happen.

The complete process is therefore described by the BKE

$$\partial_t f(t, \mathbf{n}^-, \mathbf{n}^+) = L_{\text{rep}}f(t, \mathbf{n}^-, \mathbf{n}^+) + L_{\text{prop}}f(t, \mathbf{n}^-, \mathbf{n}^+), \quad (\text{SM.35})$$

that takes into account the stochastic behavior of particles on a lattice subject to reproduction, competition, and active propulsion.

Proceeding as before, we let $\rho_i^\pm = Ln_i^\pm/N$ and similarly $\rho_0 = Ln_0/N$ to obtain

$$\begin{aligned}
L_{\text{rep}}f(t, \rho^-, \rho^+) &= \frac{\alpha}{\epsilon} \sum_{i=0}^L (\rho_i^+ (f(t, \rho^-, \rho^+ + \epsilon e_i) - f(t, \rho^-, \rho^+))) && \text{(birth of right-mover)} \\
&+ \frac{\alpha}{\epsilon} \sum_{i=0}^L (\rho_i^- (f(t, \rho^- + \epsilon e_i, \rho^+) - f(t, \rho^-, \rho^+))) && \text{(birth of left-mover)} \\
&+ \frac{\alpha}{\epsilon} \sum_{i=0}^L \left(\frac{\rho_i^+ (\rho_i - 1)}{\rho_0} (f(t, \rho^-, \rho^+ - \epsilon e_i) - f(t, \rho^-, \rho^+)) \right) && \text{(death of right-mover)} \\
&+ \frac{\alpha}{\epsilon} \sum_{i=0}^L \left(\frac{\rho_i^- (\rho_i - 1)}{\rho_0} (f(t, \rho^- - \epsilon e_i, \rho^+) - f(t, \rho^-, \rho^+)) \right) && \text{(death of left-mover)}
\end{aligned} \tag{SM.36}$$

which in the limit $\epsilon \rightarrow 0$, using the WKB approximation, yields the Hamiltonian

$$\begin{aligned}
H_{\text{rep}}(\rho^-, \rho^+, \theta^-, \theta^+) &= \alpha \sum_{i=0}^N (\rho_i^+ (e^{\theta_i^+} - 1) + \rho_i^- (e^{\theta_i^-} - 1)) && \text{(births)} \\
&+ \alpha \sum_{i=0}^N (\rho_i^+ \rho_i (e^{-\theta_i^+} - 1) / \rho_0 + \rho_i^- \rho_i (e^{-\theta_i^-} - 1) / \rho_0) && \text{(deaths)}
\end{aligned} \tag{SM.37}$$

so that in the spatial continuum limit, $h \rightarrow 0$,

$$\begin{aligned}
\mathcal{H}_{\text{rep}}[\rho^-, \rho^+, \theta^-, \theta^+] &= \alpha \int_{\Omega} (\rho^+ (e^{\theta^+} - 1) + \rho^- (e^{\theta^-} - 1)) dx && \text{(births)} \\
&+ \alpha \int_{\Omega} (\rho \rho^+ (e^{-\theta^+} - 1) / \rho_0 + \rho \rho^- (e^{-\theta^-} - 1) / \rho_0) dx. && \text{(deaths)}
\end{aligned} \tag{SM.38}$$

Taking again the canonical transformation (SM.11) gives

$$\begin{aligned}
\mathcal{H}_{\text{rep}}[\rho, \eta, \theta, \zeta] &= \int_{\Omega} \left(\frac{1}{2}(\rho + \eta) (e^{\theta + \zeta} - 1) + \frac{1}{2}(\rho - \eta) (e^{\theta - \zeta} - 1) \right) dx \\
&+ \int_{\Omega} \left(\frac{1}{2}\rho(\rho + \eta) (e^{-(\theta + \zeta)} - 1) / \rho_0 + \frac{1}{2}\rho(\rho - \eta) (e^{-(\theta - \zeta)} - 1) / \rho_0 \right) dx.
\end{aligned} \tag{SM.39}$$

To leading order with the above scaling assumptions, and rescaling $\alpha \rightarrow \tau\alpha$, the full Hamiltonian $\mathcal{H} = \mathcal{H}_{\text{prop}} + \mathcal{H}_{\text{rep}}$ finally reads

$$\mathcal{H}[\rho, \theta] = \int_{\Omega} \left(\theta \partial_x (\mathcal{D}_e \partial_x \rho - \rho D(\rho) \partial_x (\delta^2 \partial_x^2 \rho + \theta)) + \alpha \rho (e^{\theta} - 1) + \alpha \frac{\rho^2}{\rho_0} (e^{-\theta} - 1) \right) dx. \tag{SM.40}$$

4. Large deviation principle. The rate function $I_T[\rho]$ for a LDP is usually written in terms of the *Lagrangian* $\mathcal{L}[\rho, \partial_t \rho]$ [21] via

$$I_T[\rho] = \int_0^T \mathcal{L}[\rho, \partial_t \rho] dt. \tag{SM.41}$$

Since the Fenchel-Legendre transform of the full Hamiltonian \mathcal{H} of (SM.40) to obtain \mathcal{L} is very unwieldy, instead we choose to write

$$I_T[\rho] = \int_0^T \mathcal{L}[\rho, \partial_t \rho] dt = \sup_{\theta} \int_0^T \left(\int_{\Omega} \theta \partial_t \rho dx - \mathcal{H}[\rho, \theta] \right) dt = \sup_{\theta} \int_0^T \int_{\Omega} \theta \partial_t \rho dx dt \tag{SM.42}$$

in the main text's equation (4), where in the last step we used the fact that $\mathcal{H}[\rho, \theta] \rightarrow 0$ in the limit $T \rightarrow \infty$. This amounts to solving the Hamilton's equations of the associated stochastic field theory, instead of minimizing the action functional explicitly. The *instanton* equation, corresponding to equation (5) in the main text,

$$\partial_t \rho = \frac{\delta \mathcal{H}[\rho, \theta]}{\delta \theta} = \partial_x (\mathcal{D}_e \partial_x \rho - \rho D(\rho) \partial_x (\delta^2 \partial_x^2 \rho + 2\theta)) + \alpha \rho e^{\theta} - \alpha \rho^2 e^{-\theta} / \rho_0 \tag{SM.43}$$

then connects the conjugate momentum θ to the field ρ . Note that the LLN equation (i.e. the noise free mean field description) can be obtained from this equation by setting $\theta = 0$:

$$\partial_t \rho = \partial_x (\mathcal{D}_e \partial_x \rho - \delta^2 \rho D(\rho) \partial_x^3 \rho) + \alpha \rho - \alpha \rho^2 / \rho_0 \tag{SM.44}$$